Dispersive optical-model and coupled-channels descriptions of neutron scattering from ^{27}Al and ^{59}Co up to 80 MeV

M. M. Nagadi,* C. R. Howell, W. Tornow, G. J. Weisel,† M. A. Al-Ohali,* R. T. Braun, H. R. Setze,‡ Zemin Chen,§ and R. L. Walter
Department of Physics, Duke University, Durham, North Carolina 27708, USA
and Triangle Universities Nuclear Laboratory, Durham, North Carolina 27708, USA

J. P. Delaroche and P. Romain
Commissariat à l'Energie Atomique, Service de Physique Nucléaire, DAM/DIF/DPTA Boîte Postale 12, 91680 Bruyères-le-Châtel, France

(Received 23 September 2002; revised manuscript received 14 July 2003; published 31 October 2003)

Differential cross sections $\sigma(\theta)$ and analyzing powers $A_y(\theta)$ have been measured for neutron scattering from ^{27}Al and ^{59}Co at 15 MeV at the Triangle Universities Nuclear Laboratory using standard time-of-flight techniques. In addition, $\sigma(\theta)$ was measured for ^{59}Co at 10, 12, 14, 17, and 19 MeV. Two large databases covering the energy range from 0.1 to 80 MeV were formed for these nuclei from this new data and previously published data, including that for the total cross section σ_T. These sets of data were analyzed using spherical dispersive optical-model (DOM) potentials, as well as coupled-channels model (CCM) potentials. The ^{59}Co DOM gives good agreement with the $\sigma(\theta)$ data, except in the region of the first minimum. It also gives a reasonable description of our $A_y(\theta)$ measurement. The ^{27}Al DOM gives good agreement with the data, except for $\sigma(\theta)$ at backward angles below 9.4 MeV and for σ_T, for which there is up to 5% disagreement in the 10–50 MeV range. Compared to the DOM, the ^{59}Co CCM calculations give improved agreement with the $\sigma(\theta)$ data, especially at the first minimum. The σ_T calculations agree with the data to within about 3% above 1.0 MeV. The three-level CCM calculations for ^{27}Al give excellent agreement with the entire database.

DOI: 10.1103/PhysRevC.68.044610 PACS number(s): 24.10.Ht, 25.40.Dn, 24.70+s, 28.20.Cz

I. INTRODUCTION

The present measurements of differential cross sections $\sigma(\theta)$ and analyzing powers $A_y(\theta)$ for $n+^{27}$Al and $n+^{59}$Co were motivated by three considerations: to provide more extensive databases for these reactions, to develop high-quality optical potentials, and to enable a study of the nucleon-nucleus spin-spin interaction. The present measurements were conducted in energy ranges where data were nonexistent. For ^{27}Al, we measured $\sigma(\theta)$ and $A_y(\theta)$ at 15.43 MeV. For ^{59}Co, we obtained $\sigma(\theta)$ data at 9.95, 11.94, 13.93, 15.43, 16.88, and 18.86 MeV and $A_y(\theta)$ data at 15.27 MeV. Such data were needed to confirm the smooth energy dependence of these two scattering systems in these energy ranges.

We desired new optical-model potentials to provide reliable descriptions of neutron elastic scattering and total cross sections at relatively low energies, from 0.1 to 80 MeV, in keeping with earlier work of the Triangle Universities Nuclear Laboratory (TUNL) [1,2]. For both nuclear systems, we produced fits with the dispersive optical model (DOM) that are just as good as those produced with a conventional optical model. Our objective here is to extend the acceptance of the DOM approach for interpreting scattering data, including data for deformed nuclei. The $n+^{27}$Al and $n+^{59}$Co DOM analyses at positive energies follow the approach of other analyses conducted at TUNL [3,4]. Our style of DOM follows that of Mahaux and co-workers [5] except for a different choice of energy dependence for the surface imaginary term.

Because both ^{27}Al and ^{59}Co are deformed nuclei, a comparison of the DOM predictions with those of a coupled-channels model (CCM) is of interest. In the CCM analyses, we used the rotational model. For both nuclei, we investigate a simple one-level model that explicitly includes the reorientation matrix element of the ground state. For the $n+^{27}$Al system, we also consider a standard CCM in which the $\frac{5}{2}^+$, $\frac{7}{2}^+$, and $\frac{9}{2}^+$ members of the ground-state rotational band form the coupling basis. For $n+^{59}$Co, we restrict our attention to a one-level CCM, since a rotational model offers only a rough approximation for this system.

The third motivation for the present study is that reliable, energy-dependent models in the low-energy regime provide a means to interpret spin-spin cross-section data. A large amount of spin-spin total cross-section data has been obtained in measurements of the transmission of polarized neutron beams through polarized targets of ^{27}Al and ^{59}Co. In a separate paper, we report on new determinations of the strength of the spin-spin potential V_{ss} obtained with the present optical-model potentials [6]. The work presented in this paper is based in part on a doctorate dissertation Ref. [7].

*Permanent address: Department of Physics, King Fahd University of Petroleum and Minerals, Dhahran, Saudi Arabia.
†Permanent address: Department of Physics, Penn State Altoona, Altoona, PA 16601.
‡Permanent address: Department of Physics, Pearl River Community College, Poplarville, MS 39470-2201.
§Permanent address: Department of Physics, Tsinghua University, Beijing, China.

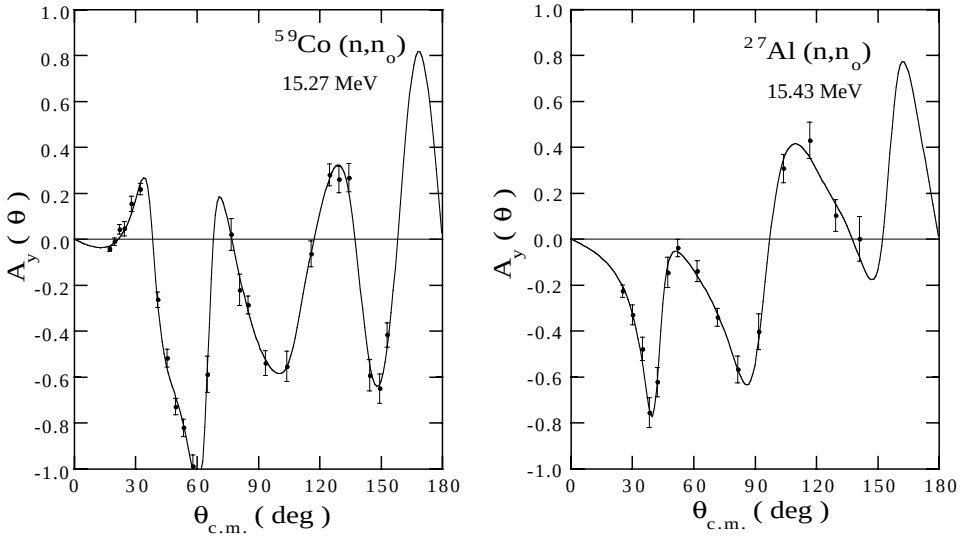

FIG. 1. The analyzing power data for ^{59}Co at E_n=15.27 MeV and for ^{27}Al at E_n=15.43 MeV. The curves are the associated Legendre polynomial fits.

II. EXPERIMENTAL TECHNIQUE

The differential cross section $\sigma(\theta)$ and analyzing power $A_y(\theta)$ for ^{27}Al and ^{59}Co were measured using the time-of-flight (TOF) facility at TUNL. Both $A_y(\theta)$ and $\sigma(\theta)$ measurements used the same apparatus except the ion source. Some of the data acquisition techniques were also identical. Only general descriptions of the equipment and the data collection procedures are given below since they already have been detailed in previous publications as indicated below.

The neutron beam was produced using the ^{2}H$(d,n)^3$He source at a reaction angle of 0° with a neutron energy spread of about 200 keV for the $\sigma(\theta)$ measurements and 400 keV for the $A_y(\theta)$ measurement. For the $A_y(\theta)$ measurements the incident deuteron beam was polarized in the TUNL atomic-beam polarized-ion source [8]. In this case, the average current of the pulsed beam on the target was 0.4 μA. Both scattering samples were cylindrical in shape and had purity greater than 99.9%.

The general layout of the neutron TOF system is described by El-Kadi [9]. For the cross-section measurements four liquid organic scintillators were used. Two of the detectors, another with a maximum flight path of 4 m and one with a maximum of 6 m, were the primary detectors and were heavily shielded. A third detector viewed the neutron production source from above and served as a monitor. A fourth detector, located at 0°, monitored the time distribution of the source neutrons. For the analyzing power measurements only three detectors were used, the 4- and 6-m detectors and the 0° detector. For the $\sigma(\theta)$ measurement, the time resolution was adequate to distinguish the elastic scattering peak from the inelastic contributions. For the $A_y(\theta)$ measurement the resolution was poorer; however, this did not matter because a narrow window could be used in selecting valid elastic scattering counts since only a ratio of the yields for the two spin orientations (spin up and spin down) is required.

The $\sigma(\theta)$ data were collected at angles between 18° and 160° in 4° steps. Measurements with a polyethylene scatterer were made to provide an absolute normalization through the known *n-p* scattering cross sections. Corrections were applied to the $\sigma(\theta)$ data for finite geometry, flux attenuation, and multiple scattering using the Monte-Carlo computer code EFFIGY15 as revised by Pedroni [10]. Relative uncertainties on the final $\sigma(\theta)$ values varied between 2% and 8%, and normalization uncertainties were about 4%. The $\sigma(\theta)$ values are listed in Ref. [7].

The $A_y(\theta)$ data were recorded in larger angular increments since the data accumulation period at a specific angle was about five times greater with the polarized beam. The data were corrected using a Monte Carlo iterative approach to calculate the effective analyzing power for the experimental conditions. For this calculation we used the computer code JANE [11], which estimates the corrections for finite geometry, neutron flux attenuation, and multiple scattering. The sizes of these corrections are displayed in Ref. [7] and the final corrected values for $A_y(\theta)$ are tabulated there. The relative uncertainties on $A_y(\theta)$ are about ±5%. There is a scale uncertainty of about ±3% associated with the determination of P_n. Figure 1 shows the $A_y(\theta)$ data alongside curves that were obtained when an expansion in terms of Legendre polynomials was fit to the product of $\sigma(\theta)$ and the measured $A_y(\theta)$.

To obtain the above $A_y(\theta)$ data the polarization of the neutron beam had to be determined. Since the atomic-beam polarized-deuteron ion source did not have a spin polarimeter at the time these data were obtained, it was decided to use $n+^{12}$C scattering as a polarimeter for the 15-MeV neutrons. We chose the laboratory scattering angle of 50°, an angle where the analyzing power is relatively large and was previously measured at TUNL [12]. [This measurement was repeated later at TUNL and the original value of $A_y(50°)$ was authenticated.] The code JANE was also used iteratively to determine corrections to the ^{12}C data. The average neutron beam polarization P_n was determined to be 0.54±0.02.

III. DATABASES AND COMPOUND NUCLEUS CALCULATIONS

The databases used in the optical-model analyses presented below are listed in Tables I and II. The model calculations describe $\sigma(\theta)$ and $A_y(\theta)$ for direct elastic scattering

TABLE I. The ^{59}Co database used to develop the DOM and CCM.

Energy (MeV)	Reference
Differential cross section	
18 energies between 1.4 and 9.5 MeV	[13]
8.97	[14]
9.95, 11.94, 13.94, 15.43, 16.88, 18.86	Present work
11.00	[15]
21.6	[16]
23.0	[17]
Analyzing power	
15.43	Present work
23.00	[17]
Total cross section	
0.04–32.0	[18]
0.5–32.0	[19]
5.0–80.0	[35]

processes, i.e., shape-elastic scattering (SE). At low energies compound-nucleus elastic scattering (CE) processes contribute to the observed elastic cross section, giving $\sigma_{EL}(\theta) = \sigma_{CE}(\theta) + \sigma_{SE}(\theta)$. At neutron energies E_n where the data of the present measurement were obtained ($E_n > 9$ MeV), the $\sigma_{CE}(\theta)$ was negligible; however, the $\sigma(\theta)$ databases used in the optical-model analyses extended into regions where σ_{CE} was important. All the $A_y(\theta)$ data were for $E_n > 10$ MeV, so the CE processes were of no concern for these data.

The $\sigma_{CE}(\theta)$ was calculated using the formalism of Hauser and Feshbach and the constant-temperature formula to model the continuum of excited states. At TUNL the computer code OPSTAT, which was modified by Das [29] to include the DOM formalism, was used in the early calculations of Ref. [7]. For the more recent calculations presented here, the DOM option of the computer code ECIS98 of Raynal [30] was used. The CN components are calculated using the width fluctuation factor due to Moldauer [31]. The DOM parameter set used to predict σ_{CE} for the final analyses was a result of several iterations of describing the CN (type designation for van de Graaff electrostotic accelerator) corrected $\sigma(\theta)$ data at low energies plus all the higher energy $\sigma(\theta)$ data. (The optimum model was determined by viewing the qualitative agreement of the calculations with the entire database.)

TABLE II. The ^{27}Al database used to develop the DOM and CCM.

Energy (MeV)	Reference
Differential cross section	
2.47, 3.0, 3.49, 4.0, 4.56, 6.09, 7.05, 8.05	[20]
7.62	[21]
9.0	[14]
10.16	[20]
11.0, 14.0, 17.0	[23]
15.43	Present work
18.0, 20.0, 22.0, 25.0, 26.0	[24]
21.6	[16]
Analyzing power	
14.0, 17.0	[25]
15.43	Present work
Total cross section	
0.2–49.0	[26]
2.0–81.0	[27]
0.5–32.0	[19]
5.0–80.0	[28]

IV. THE DISPERSIVE OPTICAL-MODEL ANALYSIS

The DOM provides a more realistic description of low-energy elastic scattering than a conventional optical model. An early study pointed out that the DOM supplies a small "bump" in the central field strength at low energies that is required by the elastic scattering data but is not attainable by conventional spherical optical models [32]. The DOM also allows extrapolation to the negative-energy regime and the prediction of bound-state quantities. In the present study, we have not attempted to extract the bound-state information, since single-particle states are not well defined for ^{27}Al and ^{59}Co.

In dispersive optical-model analyses, the real central potential is defined through the superposition of two components. The first one is called the Hartree-Fock (HF) term which is given the phenomenological form

$$\mathcal{V}_{HF}(r, E) = V_{HF}(E) f(r, a_{HF}, R_{HF}), \tag{1}$$

where $f(r, a_{HF}, R_{HF})$ is a Woods-Saxon shape. The $V_{HF}(E)$ is the energy-dependent potential depth

$$V_{HF}(E) = A_{HF} \exp[-\lambda(E - E_F)], \tag{2}$$

in which E_F is the Fermi energy. The second component is the so-called dispersive term

$$\Delta\mathcal{V}(r, E) = \frac{1}{\pi} P \int_{-\infty}^{+\infty} \frac{\mathcal{W}(r, E)}{E' - E} dE', \tag{3}$$

where P stands for principal value and $\mathcal{W}$ is the absorptive potential (assumed symmetric around E_F) which generally includes both surface ($\mathcal{W}_s$) and volume ($\mathcal{W}_v$) components. These components are defined, respectively, as

$$\mathcal{W}_s(r, E) = 4 i a_s W_s(E) \frac{d}{dr} f(r, a_s, R_s) \tag{4}$$

and

$$\mathcal{W}_v(r, E) = W_v(E) f(r, a_{HF}, R_{HF}). \tag{5}$$

Finally, the neutron OMP $U(r, E)$ used for solving the Schrödinger equation in the continuum is

$$-U(r,E) = \mathcal{V}_{HF}(r,E) + \Delta\mathcal{V}(r,E) + i\mathcal{W}_s(r,E) + i\mathcal{W}_v(r,E) + 2\lambda_\pi^2 V_{so}(\vec{l}\cdot\vec{\sigma})\frac{1}{r}\frac{d}{dr}f(r,a_{so},R_{so}). \quad (6)$$

The last term of Eq. (6) defines the nuclear spin-orbit OMP component. Note that the spin-orbit interaction is taken to be real in the present analysis. From other neutron work it is known that the imaginary part of this OMP term is small and might even be zero at the low neutron energies where the analyzing power data exist. Unfortunately, the available data for ^{59}Co and ^{27}Al are not accurate enough to assign a strength to this imaginary term.

The imaginary potential strengths are given the forms

$$W_s(E) = \frac{A_s(E-E_F)^m}{(E-E_F)^m + (B_s)^m}\exp(-C_s|E-E_F|^q) \quad (7)$$

and

$$W_v(E) = \frac{A_v(E-E_F)^n}{(E-E_F)^n + (B_v)^n}. \quad (8)$$

The Fermi energy E_F is evaluated in terms of neutron separation energies S_n as $E_F = \frac{1}{2}[S_n(N) + S_n(N+1)]$. For ^{27}Al, $E_F = -10.392$ MeV and for ^{59}Co, $E_F = -8.979$ MeV. The E-dependent potential strength in Eq. (7) is unique in its use of the factor q. This is a phenomenological factor but, as shown in the present study and an earlier TUNL study, it achieves high-quality global agreement with the available $\sigma(\theta)$, $A_y(\theta)$, and σ_T up to 80 MeV [33]. Mahaux and Sartor [5] have suggested two modifications to the imaginary potential strengths: that the strengths be zero for a small region near the Fermi energy and that the strengths used in the dispersion relation take account of the nonlocality of the imaginary potential. However, as a number of studies show [3], these modifications introduce insignificant changes to a DOM for $0 < E_n < 80$ MeV and so are not considered in the present study.

For ^{59}Co the search was initiated with the SOM parameters of Pedroni *et al.* [1]. For ^{27}Al the search was initiated with the SOM parameters of Martin [34]. A grid search method was used with the code ECIS98, which contains the electromagnetic spin-orbit interaction, i.e., the Mott-Schwinger interaction. Relativistic kinematics is used throughout.

The final DOM potential parameters are listed in Table III for ^{59}Co and ^{27}Al. In Fig. 2 we present the $\sigma(\theta)$ results for ^{59}Co. Our new data between 9.95 and 18.86 MeV are indicated by solid squares. This figure also displays the DOM calculations (dotted curves), with compound-nucleus contributions included below 8.03 MeV. The overall agreement between the predictions and measurements is quite satisfactory except at the first minimum, where in three energy regions the calculations fall below the data. Figure 3 shows the DOM calculations compared to our $A_y(\theta)$ data (stars) at 15.27 MeV and to other data at 23.00 MeV. At 15 MeV, there are differences between the data and the calculations; the phasing is correct but the calculations lay above the $A_y(\theta)$ data around 60° and 100°. [The sharp negative excursion of the calculation of $A_y(\theta)$ near 1° is caused by the Mott-Schwinger interaction.] At 23.00 MeV, the agreement is reasonable, except for angles near 30°, where the DOM gives a large negative excursion. The data of Ref. [17] probably are not able to render a narrow feature in the analyzing power, due both to limitations of angular resolution in the experiment and details of the multiple-scattering calculations (particularly concerning the narrowness and depth of the first minimum in the differential cross section). Figure 4 shows the ^{59}Co DOM calculation (dotted curve) for σ_T compared to high-accuracy measurements performed at LANL from 5 to 80 MeV [35] and to earlier measurements below 5 MeV. (Note the offset from zero for the ordinate.) The calculated σ_T lies below the data by 2% to 5% in the region from 15 to 40 MeV and somewhat above the averages of the data in the resonance region between 0.2 and 2.0 MeV.

TABLE III. Dispersive optical-model potential parameters. Energy and depths are in MeV. Geometries and lengths are in fm.

$n+^{27}$Al
$A_{HF}=51.163$; $\lambda=0.606\times10^{-2}$; $a_{HF}=0.66$; $r_{HF}=1.19$
$A_s=8.5$; $B_s=6.98$; $C_s=0.186\times10^{-3}$; $m=6$; $a_s=0.50$; $r_s=1.28$
$A_v=13.0$; $B_v=80.0$; $n=4$; $E_F=-10.392$; $q=2.0$
$V_{so}=5.7$; $a_{so}=0.41$; $r_{so}=1.00$
$n+^{59}$Co
$A_{HF}=52.50$; $\lambda=0.8\times10^{-2}$; $a_{HF}=0.74$; $r_{HF}=1.198$
$A_s=9.8$; $B_s=10.8$; $C_s=0.28\times10^{-3}$; $m=6$; $a_s=0.48$; $r_s=1.29$
$A_v=11.1$; $B_v=105.0$; $n=2$; $E_F=-8.979$; $q=2.0$
$V_{so}=5.0$; $a_{so}=0.60$; $r_{so}=1.017$

Figure 5 shows that the DOM calculations (dotted curves) for ^{27}Al describe the $\sigma(\theta)$ data quite well above 8.05 MeV except for discrepancies at the backward angles with our new data at 15.43 MeV. The calculated $\sigma_{CE}(\theta)$ has been added to the DOM calculations below 9.4 MeV. For energies below 9.4 MeV the calculations in Fig. 5 underestimate $\sigma(\theta)$ at angles from 90° to 140°. The new $A_y(\theta)$ data at 15.43 MeV are shown in Fig. 5 along with other available measurements; the data appear to be consistent with the earlier measurements. All the $A_y(\theta)$ data agree with the DOM calculations (dotted curves) except in the region near 85°, where the magnitudes of the DOM values are too small and the minimum is shifted by about 7°. Figure 6 shows the ^{27}Al DOM calculations (dotted curves) for σ_T along with the experimental data. The calculations and the measurements are in fair agreement between 100 keV and 10 MeV, as well as between 50 and 80 MeV. In the range $10 < E < 50$ MeV the DOM predictions are low, having a maximum deviation of 5% near 30 MeV.

Since our analysis was completed, two optical models have been reported in the literature that pertain to the present study: a DOM analysis for $n+^{27}$Al, Ref. [37], and a global conventional optical model, Ref. [36]. These models use data bases that include the high-energy regime, up to 250 MeV and 200 MeV, respectively. In the present study, we focused on relatively low energies and so did not wish to weight our models with high-energy data. In part, this is due to the fact

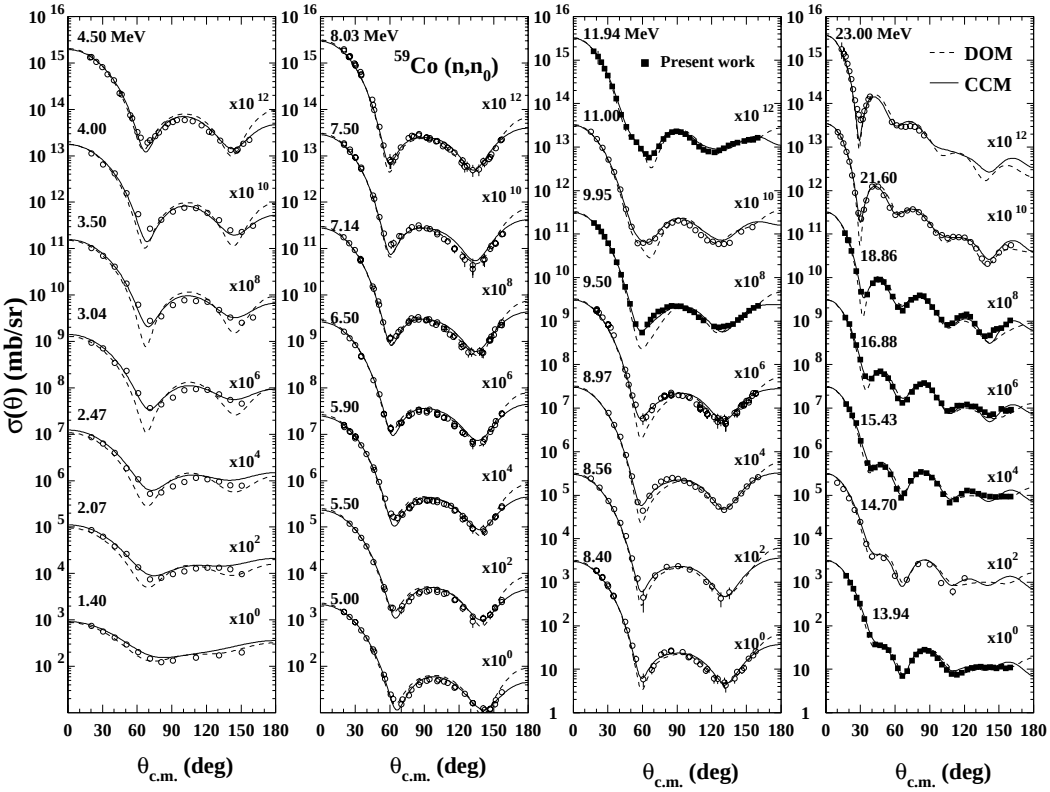

FIG. 2. Coupled-channels calculations of $\sigma(\theta)$ for ^{59}Co compared to data and to DOM calculations.

that our study is linked to a second study on spin-spin cross sections, which requires a careful determination of the energy dependence of optical models in the low-energy regime. Overall, neither Ref. [37] nor Ref. [36] yield improved fits below 80 MeV.

A more detailed comparison between the ^{27}Al DOM of the present study and that of Molina *et al.* [37] is worthwhile. The energy dependences of the two models differ: whereas Ref. [37] chose $n=m=4$ and $q=1$, we favored $n=4$, $m=6$, and $q=2$. In comparing the calculations of the two models to the $\sigma(\theta)$ data, one notes that the DOM of Ref. [37] gives a better representation in the valley around 120° for energies below 9 MeV. Their calculations fill in the valley and look similar to the coupled-channel results introduced below. In regard to the $A_y(\theta)$ calculations, the present DOM gives better agree-

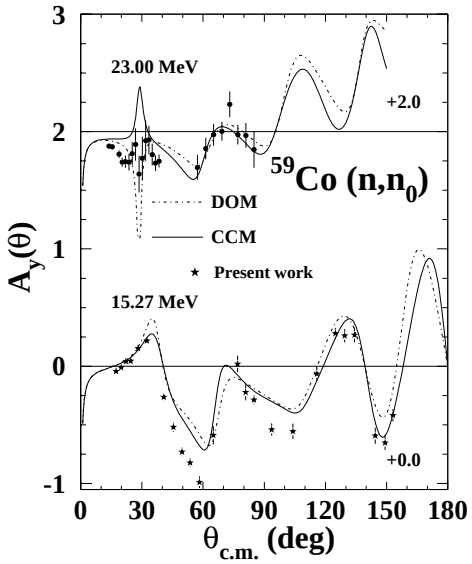

FIG. 3. Coupled-channels calculations of $A_y(\theta)$ for ^{59}Co compared to data and to DOM calculations.

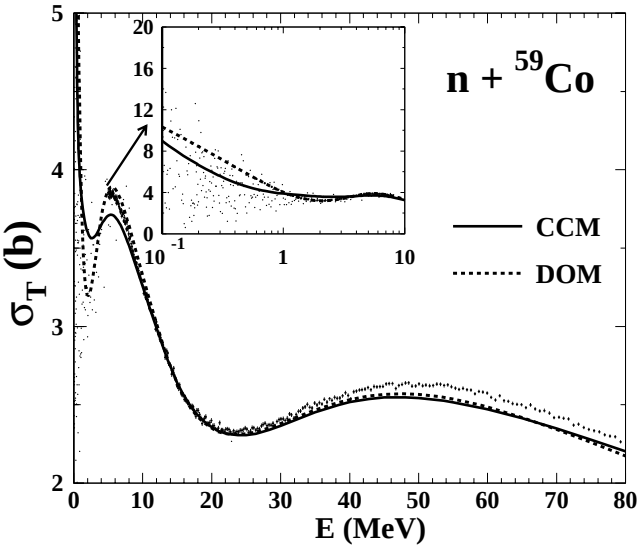

FIG. 4. Coupled-channels calculations of σ_T for ^{59}Co compared to data and to DOM calculations.

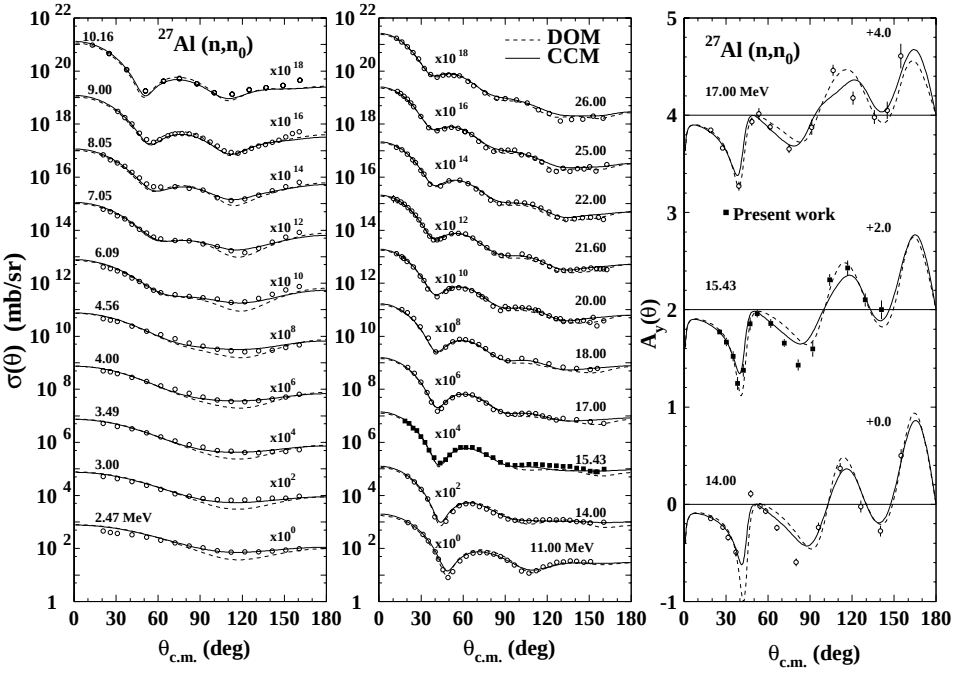

FIG. 5. Coupled-channels calculations of $\sigma(\theta)$ and $A_y(\theta)$ for ^{27}Al compared to data and to DOM calculations.

ment with the data. The DOM of Ref. [37] produces an $A_y(\theta)$ with a smaller amplitude and poorer phasing of the angles where $A_y(\theta)$ crosses through a value of zero. Considering σ_T, the DOM calculations of Ref. [37] fall at least within 2% of the data in the 15–40 MeV region where the calculations of the present DOM disagree by up to 5%.

V. THE COUPLED-CHANNELS CALCULATION

For most deformed nuclei, an analysis of scattering and reaction observables requires that the Schrödinger equation be solved in the coupled-channels framework [38]. The CCM is particularly important for achieving a successful description of neutron-nucleus interaction properties at low incident energies ($E_n < 10$ MeV), especially for the total cross section and for average resonance parameters [39].

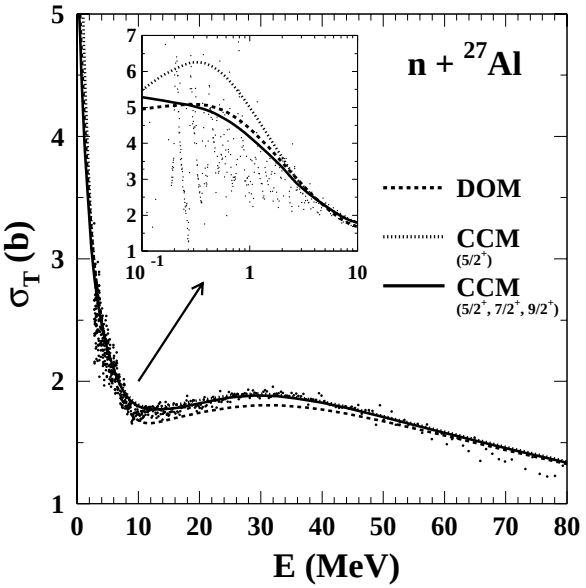

FIG. 6. Coupled-channels calculations of σ_T for ^{27}Al compared to data and to DOM calculations.

In the present analyses of the $n+^{27}$Al and $n+^{59}$Co interactions, we adopt a rotational model. A detailed discussion of rotational nuclei is given in Ref. [40]. Although this is a reasonable assumption for ^{27}Al, the level scheme of ^{59}Co suggests a vibrational structure. However, a vibrational scheme is difficult to analyze in a CCM approach, especially in the absence of available (n,n') data. We use the rotational model for ^{59}Co as a rough approximation and consider coupling only between the ground state and itself. In doing this, we demonstrate an upper limit of the reorientation effect (since the actual quadrupole moment would result in weaker coupling). The CCM calculations are performed again using ECIS98, a code which includes the full Thomas form of the spin-orbit potential and the electromagnetic spin-orbit interaction, which may be treated either as a spherical or a deformed OMP component in the calculations.

We adopted a neutron potential of the form

$$-U(\vec{r},E) = V(E)f(r,a_v,R_v) + iW_v(E)f(r,a_v,R_v) - 4ia_sW_s(E)\frac{d}{dr}f(r,a_s,R_s) + 2i\lambda_\pi^2 V_{so}\vec{\nabla}f(r,a_{SO},R_{SO}) \times \vec{\nabla}\cdot\vec{s}, \qquad (9)$$

where f is a Woods-Saxon shape in which the radius R_i depends upon deformation parameters β_λ according to

$$R_i = r_i A^{1/3}\left[1 + \sum_\lambda \beta_\lambda Y_\lambda(\Omega')\right]. \qquad (10)$$

The $V(E)$, $W_s(E)$, and $W_v(E)$ energy dependencies follow Eqs. (2), (7), and (8), respectively. The Ω' refers to the

TABLE IV. The deformed potential parameters. Energies and depths are in MeV. Geometries and lengths are in fm.

$n+^{27}$Al (one-level coupling)
$A_{HF}=55.61$; $\lambda=0.541\times10^{-2}$; $a_v=0.65$; $r_v=1.15$
$A_s=10.413$; $B_s=12.98$; $C_s=1.86\times10^{-2}$; $a_s=0.58$; $r_s=1.25$
$m=6$; $E_F=-10.392$; $q=1.0$
$A_v=9.13$; $B_v=50.0$; $n=4$
$V_{so}=6.0$; $a_{so}=0.50$; $r_{so}=1.01$
$\delta_2=-1.2075$; $\delta_4=+0.6900$
$n+^{27}$Al (three-level coupling)
All parameters are the same as above except:
$A_s=8.413$; $B_s=8.98$; $A_v=8.23$
$n+^{59}$Co (one-level coupling)
$A_{HF}=58.83$; $\lambda=0.78\times10^{-2}$; $a_v=0.65$; $r_v=1.165$
$A_s=8.53$; $B_s=10.231$; $C_s=1.08\times10^{-2}$; $a_s=0.593$; $r_s=1.261$
$m=4$; $E_F=-8.979$; $q=1.0$
$A_v=8.612$; $B_v=52.589$; $n=4$
$V_{so}=6.2$; $a_{so}=0.60$; $r_{so}=1.017$
$\delta_2=+0.952$; $\delta_4=0$

intrinsic coordinate system. In the present analyses, the deformation lengths $\delta_\lambda=\beta_\lambda R_i$ take on values that are identical for each of the deformed OMP components. The δ_λ factors were used with $\lambda=2$ and 4 in the case of ^{27}Al and $\lambda=2$ in the case of ^{59}Co. Finally, the deformed OMP components in Eq. (9) are expanded into spherical harmonics

$$U(r,\Omega')=\sum_{\Lambda}U_\Lambda(r)Y^0_\Lambda(\Omega'), \tag{11}$$

with $\Lambda=0,2,4$ for ^{27}Al and $\Lambda=0,2$ for ^{59}Co.

For even-even nuclei, a one-level CCM calculation results in no coupling at all. This is not true for $I>\frac{1}{2}$ target nuclei because the so-called reorientation matrix elements of the collective transition operator (i.e., its diagonal components in the target-spin space) used for solving the CCM equations have nonzero values. For the $\Lambda=2$ transition, the reorientation matrix element is proportional to the mass quadrupole moment of the target nucleus [41].

One-level studies are performed for neutrons incident on both ^{27}Al and ^{59}Co targets to explore the comparative figures of merit of both dispersive (spherical) and nondispersive (deformed) optical-model potentials in this medium mass range. Three-level CCM calculations are performed only for ^{27}Al, mainly for achieving good fits to $\sigma_T(E)$ at energies down to 100 keV. For that purpose, the coupling scheme adopted is $(\frac{5}{2}^+,\frac{7}{2}^+,\frac{9}{2}^+)$.

The final CCM potential parameters are listed in Table IV for ^{59}Co and ^{27}Al. We find that the CCM yields small improvements in comparison to the DOM. This is not surprising since the CCM contains one additional free parameter. In Fig. 2 it can be seen that for ^{59}Co the CCM calculations (solid curves) are in excellent agreement with the $\sigma(\theta)$ data at all energies. Our new $\sigma(\theta)$ data are particularly well described by the CCM. Figure 3 shows the DOM calculations compared to our $A_y(\theta)$ data (stars) at 15.27 MeV and to other data at 23.00 MeV. At 15.27 MeV, the CCM calculation for $A_y(\theta)$ looks similar to the DOM calculation (dotted curve); both yield a smaller magnitude than the data near 50° and 100°. The CCM σ_T calculations (solid curve) shown in Fig. 4 agree with the data to within about 3% above 1 MeV and provide a fair representation of the energy averaged data from 0.1 to 1 MeV.

The predictions of $A_y(\theta)$ at 23.00 MeV require special discussion. The CCM prediction shows a sharp positive excursion around 30°, in contrast to the DOM prediction which shows a negative excursion. This is not a surprising contradiction, insofar as OM predictions of $A_y(\theta)$ are particularly sensitive to small changes in the model parameters in this energy and angle regime. A TUNL study of ^{28}Si and ^{32}S, Ref. [42], shows that in the region of the first diffraction minimum of the differential cross section, the analyzing power changes sign from a positive peak to a negative peak across the energy range $E_n=10$ MeV to $E_n=20$ MeV. In keeping with the systematics of Ref. [42], we expect $A_y(\theta)$ for ^{59}Co to be positive around 15 MeV but negative above 20 MeV. This is in agreement with the systematics of nuclei that neighbor ^{59}Co, which are shown in Ref. [36].

The one-level CCM calculations for ^{27}Al lead to a good representation of the differential scattering measurements; however, they lead to a systematic overestimate for σ_T below 5 MeV, as can be seen from the long-dashed curve in Fig. 6. The three-level CCM calculations for $\sigma(\theta)$ and $A_y(\theta)$ for ^{27}Al, shown in Fig. 5 as the solid curves, give improved agreement with the entire database. The three-level CCM calculations for σ_T (shown as a solid curve in Fig. 6) are an improvement over the one-level CCM below 5 MeV.

VI. SUMMARY AND CONCLUSIONS

We have reported new $\sigma(\theta)$ and $A_y(\theta)$ measurements for ^{27}Al and ^{59}Co at 15 MeV and $\sigma(\theta)$ measurements for ^{59}Co at 10, 12, 14, 17, and 19 MeV. The measurements were consistent with the systematics (and the smooth energy dependence) of previously published data for these and neighboring nuclei.

Large databases were compiled for neutron scattering from ^{27}Al and ^{59}Co for σ_T, $\sigma(\theta)$, and $A_y(\theta)$ over the energy range from 0.1 to 80 MeV. The databases were used to develop dispersive optical models for ^{27}Al and ^{59}Co. Although ^{27}Al and ^{59}Co are deformed nuclei and the DOM approach has been tested mainly for spherical nuclei, we found that the DOMs describe much of the data rather well. The CCM approach was also investigated and found to improve the description of the data for all the observables for both ^{27}Al and ^{59}Co. Both the DOMs and CCMs offer excellent descriptions of the low-energy regime. Such models can be used to interpret the spin-spin cross section, a study that we present in a forthcoming paper.

In an effort to achieve an even better description of the low-energy regime (and the σ_T data), it would be interesting to extend the CCM calculations to a model that includes the dispersion relation, thus combining our two models. Such an approach has been reported by Romain and Delaroche in a study of $n+^{181}$Ta with excellent results [43].

ACKNOWLEDGMENTS

Two of the authors (M.M.N. and M.A.A-O.) would like to acknowledge King Fahd University for Petroleum and Minerals (KFUPM) for its support, especially Dr. Fahad Al-Dakhill, the former Vice-Rector for KFUPM. One of the authors (R.L.W.) acknowledges the Service de Physique Nucléaire, Centre d'Études de Bruyères-le-Châtel, for kindly hosting an extended visit to the laboratory. We are grateful to T.B. Clegg for constructing the Atomic Beam Polarized Ion Source at TUNL. This work was supported in part by the U.S. Department of Energy, Office of High Energy and Nuclear Physics, under Grant No. DE-FG02-97ER41033. Additional support came from the China National Science Foundation (Grant No. 19275026) and from the U.S.-China Cooperative Science Program of the U.S. National Science Foundation.

[1] R. S. Pedroni, C. R. Howell, G. M. Honoré, H. G. Pfutzner, R. C. Byrd, R. L. Walter, and J. P. Delaroche, Phys. Rev. C **38**, 2052 (1988).
[2] G. M. Honore, W. Tornow, C. R. Howell, R. S. Pedroni, R. C. Byrd, R. L. Walter, and J. P. Delaroche, Phys. Rev. C **33**, 1129 (1986).
[3] G. J. Weisel, W. Tornow, C. R. Howell, P. D. Felsher, M. Al-Ohali, M. L. Roberts, R. K. Das, R. L. Walter, and G. Mertens, Phys. Rev. C **54**, 2410 (1996).
[4] Zemin Chen, R. L. Walter, W. Tornow, G. J. Weisel, and C. R. Howell (unpublished).
[5] C. Mahaux and R. Sartor, Adv. Nucl. Phys. **20**, 1 (1991).
[6] J. P. Delaroche, P. Romain, M. M. Nagadi, and R. L. Walter (unpublished).
[7] M. M. Nagadi, Ph.D. dissertation, Duke University, 1992.
[8] T. B. Clegg *et al.*, Nucl. Instrum. Methods Phys. Res. A **357**, 200 (1995).
[9] S. M. El-Kadi, C. E. Nelson, F. O. Purser, R. L. Walter, A. Beyerle, C. R. Gould, and L. W. Seagondollar, Nucl. Phys. **A390**, 509 (1982); see also S. M. El-Kadi, Ph.D. dissertation, Duke University, 1981.
[10] R. S. Pedroni, Ph.D. dissertation, Duke University, 1986.
[11] E. Woye, Ph.D. dissertation, University of Tübingen, 1983.
[12] W. Tornow, E. Woye, and R. L. Walter, J. Phys. G **13**, 177 (1987).
[13] A. B. Smith *et al.*, Nucl. Phys. **A483**, 50 (1988).
[14] D. E. Velkley *et al.*, Phys. Rev. C **9**, 2181 (1974).
[15] J. C. Ferrer *et al.*, Nucl. Phys. **A275**, 325 (1977).
[16] N. Olsson *et al.*, Nucl. Phys. **A472**, 237 (1987).
[17] S. T. Lam *et al.*, Phys. Rev. C **32**, 76 (1985).
[18] G. de Saussure *et al.*, Ann. Nucl. Energy **19**, 393 (1992).
[19] S. Cierjacks *et al.*, KFK-1000 (1968).
[20] B. Holmquist *et al.*, Nucl. Phys. **A188**, 24 (1972) and references therein.
[21] G. Dagge *et al.*, Phys. Rev. C **39**, 1768 (1989).
[22] G. Boerker *et al.*, PTB-N-1, 1989.
[23] C. S. Whisnant *et al.*, Phys. Rev. C **30**, 1435 (1984).
[24] J. S. Petler *et al.*, Phys. Rev. C **32**, 673 (1985).
[25] Ph. Martin and R. L. Walter, Phys. Rev. C **34**, 384 (1986).
[26] F. G. Perey *et al.*, ORNL-4823, 1972.
[27] D. C. Larson *et al.*, ORNL-5787, 1981.
[28] R. W. Finlay *et al.*, Phys. Rev. C **47**, 237 (1993).
[29] R. K. Das (private communication).
[30] J. Raynal (private communication).
[31] P. A. Moldauer, Nucl. Phys. **A344**, 185 (1980), and references therein.
[32] J. Rapaport, T. S. Cheema, D. E. Barnum, R. W. Finlay, and J. D. Carlson, Nucl. Phys. **A296**, 95 (1978).
[33] G. J. Weisel and R. L. Walter, Phys. Rev. C **59**, 1189 (1999).
[34] Ph. Martin, Nucl. Phys. **A466**, 119 (1987).
[35] W. P. Abfalterer, F. B. Bateman, F. S. Dietrich, R. W. Finlay, R. C. Haight, and G. L. Morgan, Phys. Rev. C **63**, 044608 (2001).
[36] A. J. Koning and J. P. Delaroche, Nucl. Phys. **A713**, 231 (2003).
[37] A. Molina, R. Capote, J. M. Quesada, and M. Lozano, Phys. Rev. C **65**, 034616 (2001).
[38] T. Tamura, Rev. Mod. Phys. **37**, 679 (1965).
[39] J. P. Delaroche, Ch. Lagrange, and J. Salvy, *Nuclear Theory in Neutron Nuclear Data Evaluation* (IAEA, Vienna, 1976), Vol. II, p. 251.
[40] J. P. Delaroche, G. Haouat, J. Lachkar, Y. Patin, J. Sigaud, and J. Chardine, Phys. Rev. C **23**, 136 (1981).
[41] C. B. Fulmer, G. R. Satchler, E. E. Gross, F. E. Bertrand, C. D. Goodman, D. C. Hensley, J. R. Wu, N. M. Clarke, and M. F. Steeden, Nucl. Phys. **A356**, 235 (1981).
[42] M. Al-Ohali, Ph.D. dissertation, Duke University, 1993.
[43] P. Romain and J. P. Delaroche, in *Proceedings of OECD/NEA Specialists' Meeting on the Nucleon Nucleus Optical Model up to 200 MeV, Bruyeres-le-Chatel, 1996*, available at http://www.nea.Fr/html/science/om200.